HHS Public Access

Author manuscript

J Phys Chem B. Author manuscript; available in PMC 2019 January 09.

Published in final edited form as:

J Phys Chem B. 2017 April 20; 121(15): 3443–3457. doi:10.1021/acs.jpcb.6b09111.

Lipid and Peptide Diffusion in Bilayers: the Saffman-Delbrück Model and Periodic Boundary Conditions

Richard M. Venable[1], **Helgi I. Ingólfsson**[2], **Michael G. Lerner**[3], **B. Scott Perrin Jr.**[1], **Brian A. Camley**[4], **Siewert J. Marrink**[2], **Frank L.H. Brown**[5], and **Richard W. Pastor**[1]

[1]Laboratory of Computational Biology, National Heart, Lung, and Blood Institute, National Institutes of Health, Bethesda, Maryland 20892, USA [2]Groningen Biomolecular Sciences and Biotechnology Institute and Zernike, Institute for Advanced Materials, University of Groningen, Nijenborgh 4, 9747 AG Groningen, The Netherlands [3]Department of Chemistry & Biochemistry and Department of Physics and Astronomy, Earlham College, Richmond, Indiana 47374, USA [4]Department of Physics, University of California, San Diego, California 92093, USA [5]Department of Chemistry & Biochemistry and Department of Physics, University of California, Santa Barbara, California 93106, USA

Abstract

The Periodic Safmann-Delbrück (PSD) model, an extension of the Safmann-Delbrück model developed to describe the effects of periodic boundary conditions on the diffusion constants of lipids and proteins obtained from simulation, is tested using the coarse-grained Martini and all-atom CHARMM36 (C36) force fields. Simulations of pure Martini dipalmitoylphosphatidylcholine (DPPC) bilayers and those with one embedded gramicidin A (gA) dimer or one gA monomer with sizes ranging from 512 to 2048 lipids support the PSD model. Underestimates of D^{∞} (the value of the diffusion constant for an infinite system) from the 512 lipid system are 35% for DPPC, 45% for the gA monomer, and 70% for the gA dimer. Simulations of all-atom DPPC and dioleoylphosphatidylcholine (DOPC) bilayers yield diffusion constants not far from experiment. However, the PSD model predicts that diffusion constants at the sizes of the simulation should underestimate experiment by approximately a factor of 3 for DPPC and 2 for DOPC. This likely implies a deficiency in the C36 force field. A Bayesian-based method for extrapolating diffusion constants of lipids and proteins in membranes obtained from simulation to infinite system size is provided.

Graphical Abstract

Email address of corresponding author: pastor@nhlbi.nih.gov, Phone number of corresponding author: 301-435-2035.

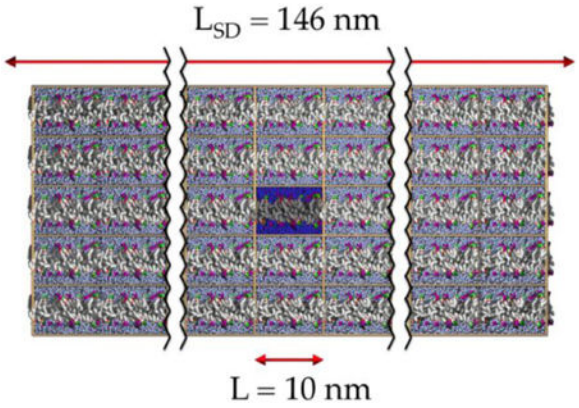

1. INTRODUCTION

Molecular dynamics (MD) simulations are typically carried out in periodic boundary conditions (PBC). This technique, wherein the primary cell is replicated and particles can pass freely between cells, affords the possibility of modeling bulk fluids or molecular assemblies such as membranes with a computationally feasible number of particles. It is intuitively obvious that behavior associated with wavelengths longer than the primary cell might be perturbed by PBC. Translational diffusion is a well-known example of dynamics extending multiple molecular lengths, and the effects of PBC in simulations of fluid flow around spheres and infinite cylinders was first presented in 1959 by Hasimoto,[1] though not in the context of simulations. More recently Dunweg and Kremer[2] and Yeh and Hummer[3] published similar predictions in the specific context of simulations for the calculation of diffusion coefficients run under PBC in homogeneous 3D systems. This PBC correction is easy to calculate and relatively small (10–20%) for self-diffusion in systems of several hundred molecules. However, as recently estimated by Camley et al.[4] using a hydrodynamic approach based on the Saffman-Delbrück (SD) model,[5] the PBC artifact for membrane systems is much more serious. Assuming that the force field (FF) for the simulation is close to correct, calculated lateral diffusion constants (D^{PBC}) of membrane spanning proteins will underestimate experiment by factors of 3–10 for system sizes presently possible with all-atom MD. Vögele and Hummer[6] have explicitly demonstrated a dramatic system size dependence for the diffusion constant of a carbon nanotube in a 1-palmitoyl-2-oleoyl-sn-glycero-3-phosphocholine (POPC) bilayer using coarse-grained simulations over a wide range of box lengths. Conversely, the length and height dimensions of the simulation cell are predicted to require increases of 10 to 100-fold to attain diffusion constants comparable to the infinite system size value (D^{∞}).

Camley et al. also developed expressions for D^{∞} and D^{PBC} for a cylinder spanning only a single leaflet, as appropriate for modeling monotopic peptides and proteins, and possibly lipids; the interleaflet friction, not present in the original SD model, is the required additional parameter. The case of lipids is germane for both practical and theoretical reasons. Statistical errors in diffusion constants calculated for lipids in simulation are significantly smaller than those of proteins because their relative populations in the bilayer are so much larger. Hence, lipid diffusion constants are superior targets for comparing with experiment

when developing force fields (FF), and it is thereby critical to describe PBC artifacts accurately. Turning to theory, the Saffman-Delbrück model has been largely accepted for large proteins for decades,[7–9] though there remains controversy for some systems.[10–12] The application of the SD model to lipids is more tenuous because it presumes the validity of hydrodynamic theories down to the scale of the individual molecules comprising the fluid. It has been argued, for example, that the chain length dependence of lipid diffusion constants are inconsistent with SD.[7, 13] However, the original SD model was developed for membrane spanning cylinders and does not include interleaflet friction, so a reevaluation in light of the half-cylinder formula of Camley et al. is warranted.

While the results of some Martini CG simulations are included in Camley et al., that study was primarily theoretical. This study presents results from coarse-grained simulations of gramicidin A (gA) dimers and monomers in dipalmitoylphosphatidylcholine (DPPC) bilayers using the Martini model, and pure DPPC bilayers, and all-atom simulations of DPPC and dioleoylphosphatidylcholine (DOPC) using the CHARMM36 (C36) force field.[14] The CG simulations allow a critical consistency check of the hydrodynamic model: whether size dependent diffusion constants for membrane spanning (gA dimer) and monotopic (gA monomers) cylinders of equal radii and pure DPPC can be described with the same membrane viscosity and interleaflet friction. The size dependence of the diffusion constants from all-atom simulations of DPPC and DOPC is also compared with the model to examine trends and to estimate hydrodynamic parameters. The simulations allow an investigation of the effects of bound solvent. Just as bound water adds to the effective hydrodynamic radii of proteins in aqueous solution,[15] it is necessary to consider the possibility that bound lipids can increase the effective radii of membrane proteins and peptides; the simulations of Niemela at al.[16] strongly suggest the presence of such bound lipids. This could be particularly important for peptides and smaller proteins, where the relative increase in radii is greater.

This study also considers the very practical question for the effect of ensemble, pressure, and temperature controls on calculated diffusion constants. Specifically, while most methods of pressure and temperature control in simulations have been shown to rigorously correspond with the associated statistical mechanical ensemble, this is not that case for transport properties; i.e., transport properties such as diffusion can only be rigorously obtained from simulation in the microcanonical (constant particle number, volume, and energy, or NVE) ensemble.[17] Given that nearly all membrane simulations are carried out at constant pressure and temperature, it is relevant to determine whether the differences with NVE are unacceptably large. Additionally, most MD programs periodically remove center of mass (COM) translation and rotation to offset energy leakage arising from numerical errors. This effect is examined by comparing diffusion constants evaluated with explicit Ewald summation[17] of electrostatic forces (where COM removal is not required) and the computationally more efficient Particle Mesh Ewald (PME)[18] (where COM removal is standard).

By way of outline, the Method section reviews the hydrodynamic model and describes the simulation protocols. The Results and Discussion contains three subsections: 3.1, a comparison of self-diffusion constants obtained from simulations of DPPC bilayers carried

out with different programs and ensembles; 3.2, a comparison of diffusion constants from coarse-grained and all-atom simulations with the hydrodynamic model; and 3.3, a comparison of the diffusion constants of DPPC and DOPC from C36 all-atom lipid parameter set and experiment. Avenues for FF improvement and general strategies for extrapolation to obtain D^{∞} are then discussed. The Appendix provides a Bayesian analysis method to estimate D^{∞} and to set bounds on extrapolated diffusion constants.

2. METHODS

2.1. Review of Theory.

The treatment of PBC in Camley et al. is developed within the framework of the Saffman-Delbrück model, which predicts that the diffusion constant of a small membrane spanning cylinder of radius R in an infinite flat membrane suspended in an infinite bulk fluid is

$$D = \frac{k_B T}{4\pi\eta_m}\left(\ln\frac{\eta_m}{\eta_f R} - \gamma\right) = \frac{k_B T}{4\pi h\eta_m^b}\left(\ln\frac{h\eta_m^b}{\eta_f R} - \gamma\right) \quad (1)$$

where η_m is the membrane surface viscosity, η_f is the bulk viscosity of the surrounding fluid, k_B is Boltzmann's constant, T is the temperature, and γ is Euler's constant.[5] The surface viscosity η_m may be thought of as a product of the membrane height h and an effective lipid bulk viscosity; the SD equation is often written in terms of (RHS side of Eq (1)). The critical physical parameter is the Saffman-Delbrück length $L_{SD} = \eta_m/2\eta_f$, which demarks the crossover point between 2D-like hydrodynamics in the membrane (at short scales) and 3D-like hydrodynamics in the membrane (at long scales). Because L_{SD} ranges from 100 nm[9] to microns[19] (depending on the system) and typical cell-sizes for all-atom simulations of membranes are about 10 nm, it is easy to surmise that PBC artifacts could be serious.

Now consider a periodic simulation cell consisting of the same cylinder in a bilayer with edge length L and water layers each of thickness H above and below (hence, if the bilayer thickness is 4 nm, the height of the cell is 4 nm + 2H). The diffusion constant in the periodic system is denoted D^{PBC}; that of the infinite system ($L \to \infty$, $H \to \infty$) is D^{∞}. Using the immersed boundary method,[20] the preceding diffusion constants for a membrane spanning cylinder are

$$D^{PBC} = \frac{k_B T}{2L^2}\sum_{k\neq 0}\frac{1}{\eta_m k^2 + 2\eta_f k\tanh(kH)}e^{-k^2\beta^2R^2/2} \quad (2a)$$

$$D^{\infty} = \frac{k_B T}{2}\int\frac{d^2k}{(2\pi)^2}\frac{1}{\eta_m k^2 + 2\eta_f k}e^{-k^2\beta^2R^2/2} \quad (2b)$$

where β = 0.828494. (This value of β is chosen to reproduce accurately the generalization of the Eq. (1) to arbitrary values of R/L_{SD} developed by Hughes, Pailthorpe, and White,[21] and Petrov and Schwille.[22]) The extension of Eqs. (2) to a single leaflet spanning cylinder requires one more parameter, the intermonolayer friction b:

$$D^{PBC} = \frac{k_B T}{2L^2} \sum_{k \neq 0} \frac{A(k)}{A(k)^2 - B(k)^2} e^{-k^2 \beta^2 R^2/2} \quad (3a)$$

$$D^{\infty} = \frac{k_B T}{2} \int \frac{d^2 k}{(2\pi)^2} \frac{A(k)}{A(k)^2 - B(k)^2} e^{-k^2 \beta^2 R^2/2} \quad (3b)$$

$$A(k) = \eta_{mono} k^2 + \eta_f k \coth(2Hk) + b$$

$$= \eta_{mono} k^2 + \eta_f k + b; \quad H \to \infty$$

$$B(k) = b + \eta_f k \operatorname{csch}(2Hk)$$

$$= b; \quad H \to \infty$$

where $\eta_{mono} = \eta_m/2$ is the monolayer surface viscosity.

For notational simplicity, Eqs. (2a) and (3a) are denoted the *Periodic Saffman-Delbrück* (PSD) model, even though they are more general than the original. https://diffusion.lobos.nih.gov provides a web-interface that evaluates D^{PBC} and D^{∞} for individual sets of parameters. See ref. 4 for complete derivations, and especially Section VI for a discussion of the limitations of the model. Vögele and Hummer[6] present an analytic approximation for the error due to PBC in membrane systems that neglects protein size and assumes $L >> H$; in the appropriate regimes they obtain good agreement with Eqs. (2).

The PSD model, as in the original work of Saffman and Delbrück, assumes a perfectly flat membrane and homogeneous Newtonian fluids (membrane and solvent) surrounding the diffusing body. Out-of-plane membrane deformations and/or in-plane membrane inhomogeneities (e.g. other proteins or lipid domains) are not considered. Vögele and Hummer[6] showed in their Martini simulations that the effect of undulations on the diffusion constant is relatively small, as predicted theoretically.[23–25]

In recent work, various groups have begun to simulate the self-diffusion of proteins and/or lipids in protein laden membranes via Martini.[26–29] Unfortunately, the influence of PBC on very crowded membranes is less clear. At low protein concentrations, self-diffusion is expected to be influenced primarily by enhancing the effective viscosity of the membrane relative to that of the pure lipid bilayer,[30–31] in analogy to the Einstein viscosity of a fluid particulate suspension in 3D.[32] Continuum level simulations[33] suggest that this picture is valid up to protein area fractions of ~10%, which implies that the PSD equations will be useful in the description of modestly concentrated protein decorated bilayers (assuming that appropriate effective membrane viscosities are used in the equations). However, direct protein-protein interactions become important at higher concentrations and may eventually overwhelm naive hydrodynamic considerations.[34–35] Given the preceding complexities, it would be advisable to carry out simulations at several system sizes to at least test for PBC effects.

As shown in Fig. 1 for $R = 3$ nm and $L_{SD} = 160$ nm, Eq. (2a) predicts that $D^{PBC} < D^{\infty}$ for all practical system sizes in all-atom simulations; it is only when both L *and* H are significantly larger than L_{SD} that a simulation reliably yields D^{∞}. Remarkably, increasing L while holding H constant eventually changes the sign of the error (i.e., $D^{PBC} > D^{\infty}$). This result implies that a simulation could, in principle, yield $D^{PBC} = D^{\infty}$ at small H; however, such a system would not correctly model a free standing bilayer. Table 1 presents diffusion constants calculated from Eqs. (2) for representative system sizes for all-atom simulations for $L_{SD} = 160$ nm (the value used to generate Fig. 1) and $L_{SD} = 78$ nm (an estimate from protein diffusion measurements in a black lipid film[8]). Underestimates are approximately a factor of 3 for the single helix transmembrane peptide WALP23 and factor of 10 for the protein galactose transferase (GltT). As discussed in ref. 4, PBC errors are smaller for the CG model because system sizes are larger and the membrane viscosity (and consequently L_{SD}) are smaller; however, they can still be substantial. (The absolute errors of the CG model relative to experiment are severe due to the underestimation of membrane viscosity and can completely overshadow the effects of PBC.)

2.2. Coarse-grained simulations.

All coarse-grain (CG) simulations were performed using the Martini model,[36–39] with the "common" parameter set of de Jong et al..[40] The topology for gramicidin (gA) monomer and dimer was derived from the gA crystal structure (PDB ID 1JNO)[41] using *martinize* v2.2 (see www.cgmartini.nl/) with ElNeDyn22.[37–39, 42] Backbone bead types were reassigned based on gA's $\beta^{6.3}$-helixes structure and the number of hydrogen-bonds in the gA crystal structure backbone. The ethanolamine groups (ETA) and formyl groups (FOR) were modeled with P2 and sN0 beads, respectively.

Simulations were carried out in both GROMACS (4.6.7)[43] and CHARMM[44] to test the sensitivity of results to different methods of temperature and pressure control. Beginning with the GROMACS set, pure DPPC bilayers were assembled with 512, 1024, 2048, 4096, 8192, and 32768 lipids with an equal number of lipids in each monolayer. Gramicidin A dimer simulations were assembled with one dimer in 512, 1024, or 2048 lipids; gA monomer simulations were of the same size except six additional DPPC lipids were added to

the monolayer-free leaflet. Figure 2 shows the small and large gA systems. All simulations were hydrated with ~33 CG waters (corresponding to ~132 water molecules) per lipid and set-up using the bilayer builder *insane*,[45] except for the 8192 and 32768 pure DPPC lipid systems which were constructed from four 2048 and 8192 lipids systems after 20 μs of simulation. Initial systems were energy-minimized (steepest descent, 500 steps) and simulated for 22 ns using short time step 1–10 fs and weak coupling (WC), also known as the Berendsen barostat.[46] For production simulations a time step of 20 fs was used for the simulations with gA and 40 fs for the pure DPPC simulations. Lennard−Jones (LJ) interactions were shifted between 0.9 and 1.2 nm, Coulomb interactions were screened by a relative permittivity constant $\varepsilon_r = 15$ and shifted to zero between 0 and 1.2 nm. The temperature was maintained at 323 K using the velocity rescaling thermostat with a relaxation time constant $\tau_T = 1.0$ ps.[47] A semi-isotropic pressure-coupling scheme was used, with a compressibility of $3{\cdot}10^{-4}$ bar^{-1}, and pressure kept at 1 bar using either weak coupling[46] with a relaxation time constant $\tau_p = 3.0$ ps or the Parrinello−Rahman barostat[48] with a relaxation time constant $\tau_p = 5.0$ ps, as indicated (see Table 2). The center of mass motion was removed separately for the bilayer and solvent phase every 100 steps and frames saved for analysis every 30000 steps.

The second set of pure-lipid CG simulations was performed in CHARMM using a domain decomposition scheme[49] (for speed enhancement) and an update[50] to run Martini without modification. NPT and NVE simulations of pure DPPC bilayers with 512 and 2048 lipids and with initial water heights of H=4.85 nm and H=9.70 nm, reported in Camley *et al.*[4] were extended for the present study (see Table 2 for trajectory lengths). Pressure (1 atm) and temperature (323 K) were controlled for NPT simulations with the Hoover barostat[51] and Nosé thermostat.[52] The center of mass motion was removed from NPT systems as a whole (combined bilayer and water) every 100 steps. COM motion was not removed from NVE systems (there was no drift). Both NPT and NVE simulations used a time step of 20 fs, and coordinates were saved for analysis every 1000 steps.

2.3. All-atom simulations.

Simulations using CHARMM were carried out using in-house computers and are described first, followed by those on Anton. The lipids and water were described by CHARMM36 (C36)[14] and modified TIP3P[53–54], respectively.

For simulations carried out with CHARMM[44] the extended system barostat[51] and thermostat[52] were employed for NPT simulations and all but one NVT simulation. In this implementation, the pressure tensor is fully anisotropic and requires a tetragonal prism simulation unit cell, where $x = y$ by constraint, with the bilayer normal vector aligned with the z axis; the cell height and the xy area are coupled to separate pistons (the same protocols were used for the CHARMM CG simulations). The NPT ensemble was generally used, except for several DPPC simulations that used NVE and NVT ensembles. One NVT simulation utilized Langevin dynamics with a collision frequency of 1 ps^{-1} to explore the effects of such a temperature control method on translational diffusion. The all-atom CHARMM simulations were run with recent (c39b2 and later) versions of the program that include a domain decomposition scheme[49] for the pairwise non-bond calculation; the

particle-particle Ewald simulations could not use this scheme. The electrostatic term was computed via Ewald methods; the particle-mesh Ewald[18] used a real space cutoff of 12 Å, a κ value of 0.32, and ca. 1 grid point per Å in each direction for the mesh. For the particle-particle Ewald, a κ value of 0.34 was used, with k-space replicas of 3,3,5 in x,y,z, a maximum k^2 setting of 50, and with the same 12 Å real space cutoff. The van der Waals dispersion term used an LJ functional form with a force-switching function over the interval of 8 to 12 Å, with a 1 fs integration time step. Endpoints from previously published simulations of 72 DPPC and DOPC lipids were used as initial conditions and to build systems of 144 and 288 lipids.

All but two of the all-atom systems contained approximately 30 waters/lipid ($H \approx 1.5$ nm), a level considered at "full hydration" as measured by structural properties such as surface area and melting point.[55,56] To allay concerns that this hydration level is insufficient for capturing the hydrodynamics of lipid diffusion, the following simulations of bilayers with 288 DPPC were generated: 3 replicates (110 ns each) with 15.2 waters/lipid ($H = 0.73$ nm), and 1 replicate of 420 ns with 60.8 waters/lipid (H=2.87 nm). Because the PSD model predicts a negligible difference in diffusion constants for these values of H (at $L = 9.5$ nm), a substantial difference would indicate that testing with additional waters is required.

Trajectories of 72, 144, and 288 DPPC and 288 DOPC were extended on the Anton super computer.[57] Each Anton trajectory was initialized with positions and velocities of the CHARMM trajectory at 50 ns. A tetragonal unit cell with x and y dimensions set to the same length and independent of the z-dimension was maintained. The temperature was maintained at 298 K for DOPC and 323 K for DPPC by the Nosé thermostat. A total pressure of 1 atm was maintained by the Martyna-Tobias-Klein barostat[58] with semi-isotropic scaling applied every 100 time steps. Long-range interactions were evaluated every time step for simulations run with CHARMM and every other time step for those run on Anton. Table 3 lists the trajectory lengths used for calculating diffusion constants (these values do not include the initial 10–20 ns deleted for equilibration).

2.4. Determination of the diffusion constant.

The COM motion of the bilayer was removed prior to computation of the mean-squared displacement (msd) for each lipid as a function of time. The msd for each lipid was computed via a difference correlation function using the x and y components of the lipid COM, after both the removal of image centering artifacts, and the bilayer COM correction. A Fortran90 program was used to compute 2D diffusion constants from the slopes of $\langle msd \rangle_{LIPIDS}$ vs time, for 10 ns $< t < (t_i - 10)/2$; t_i is the analysis time interval (ns), and the lower cutoff removes subdiffusive dynamics which is somewhat more prominent for all-atom than CG simulations (see Fig. 3).

Standard errors were estimated from replicates for the following simulations: GROMACS gA, the CHARMM CG 512 DPPC with 23.9 waters/lipid, the particle-particle Ewald, and the 288 DPPC with 15.2 waters/lipid. Block averages were used for the rest, based on an analysis as a function of the number of blocks for trends in the standard error, and upon agreement of <D> from the blocks with D obtained by fitting all of the available data. For CG models, the 10 μs CHARMM simulations used five blocks of 2 μs, while the 40 μs

GROMACS simulations used ten blocks of 4 μs. All atom systems of 200 ns or more used 4 or 5 blocks, which were often comparable; if they were not, the standard error was taken based on the agreement of <D> with D, as noted. For the shorter simulations (less than 200 ns), only three blocks were used to determine the standard error; these systems had 648 lipids, and the larger number of particles compensated for the shorter time blocks.

3. RESULTS AND DISCUSSION

3.1. Comparison of Methodology for Simulated Lipid Diffusion Constants.

This subsection focuses on the sensitivity of diffusion constants to simulation methods, and later subsections compare them with theory and experiment. The CG results are considered first because the precision of the diffusion constants (se of 0.5–1%) is higher than for the all-atom (5–10%). Table 2 lists D, their standard errors (se), and system information for DPPC based on the Martini FF using CHARMM and GROMACS; Table 3 provides the same for DPPC and DOPC from all-atom simulations based on the CHARMM36 force field using CHARMM and Anton.

As noted in the Introduction, simulations run at NVE without PME provide the most rigorous comparison with hydrodynamic theory. Hence, the 4 NVE simulations carried out in CHARMM reported in Table 2 serve as references for the CG systems. When compared with the 4 NPT simulations, the differences in D are approximately 2 se or less (the 95% confidence interval, or CI, is approximately $D \pm 2$ se). A paired t-test yields p=0.13; i.e., the differences among the diffusion constants from NVE and NPT are not statistically significant.

Pressure was controlled for Martini simulations with GROMACS using either Parrinello-Rahman (PR) or weak coupling (WC). Diffusion constants for PR and CHARMM are well within statistical error of 0.15×10^{-7} cm^2/s for N=512, but PR is a statistically significant 5% lower than CHARMM for N=2048. D for WC are 7% lower than CHARMM for both N. These results indicate that NPT simulations using GROMACS with WC can be expected to provide correct trends in diffusion constants, but that PR is preferable for quantitative estimates.

Turning to the all-atom simulations, all electrostatic energies were evaluated using PME for all but one set, which employed direct Ewald summation (where COM drift is absent and therefore does not need to be removed). Three replicates totaling 500 ns were carried out using CHARMM for N = 288, labeled NVE (Ewald) in Table 3; the 95% CI (in units of 10^{-7} cm^2/s) is 2.1–2.9. The 95% CI from CHARMM simulations at NVE with PME (1.7–2.3), and NPT with PME (1.9–2.1), and a simulation run on Anton at NPT with PME (2.2–2.4) indicate reasonable statistical equivalence among the set. The weighted average diffusion constant, $2.3 \pm 0.1 \times 10^{-7}$ cm^2/s, thereby provides an improved estimate for this system.

The preceding results indicate that simulations using CHARMM or Anton carried at NPT using extended system methods for temperature and pressure control and PME for summation of electrostatics provide an acceptable alternative to NVE with Ewald summation.

Table 3 includes the diffusion constants for simulations with H = 0.73 nm (15.2 waters/lipid), and H = 2.87 nm (60.8 waters/lipid). The results are close to those at H=1.46 nm (30.4 waters/lipid). This is consistent with the observation that there approximately 8 "structural waters" (a thickness of approximately 0.4 nm) for DPPC,[56] and that the PSD model predicts a negligible change in D in this range of H. Hence, the hydration levels are likely not a confounding factor in this study.

One of the all-atom simulations of N = 288 run with CHARMM does not group with the rest. $D = 1.5 \pm 0.1 \times 10^{-7}$ cm^2/s for NVT (LD), which is approximately 35% lower than the weighted average value of $2.3 \pm 0.1 \times 10^{-7}$ cm^2/s for the others. Here the temperature was maintained using Langevin Dynamics with a collision frequency of 1 ps^{-1}. It is not surprising that the additional damping reduces the diffusion constant, and this effect should be considered when comparing results from different programs with each other and with experiment.

3.2. Coarse-Grained Simulations

3.2.1. Comparison with the Periodic Saffman-Delbrück model.—

Table 4 lists diffusion constants for gramicidin A (gA) dimers and monomers, and lipids from CG simulations at three different values of L. The diffusion constants for lipids in the monomer mixtures all differ by less than 1% from those of the pure systems (see Table 3), and they are within a standard error of each other. Diffusion constants for lipids in the dimer systems are slightly lower than in the pure systems (3.5%, 1.7%, and 1.1% for N = 512, 1024, and 2048, respectively). These differences indicate some perturbation to the behavior of lipids close to the gA.

The evaluation of the PSD model was carried out for three sets of parameter values (Table 5). For Sets I and II the hydrodynamic parameters η_m, η_f and b obtained for the Martini model of DPPC at 323 K by den Otter and Shkulipa[59] were used without modification. The radius of DPPC for Set I was based on the well calibrated surface area/lipid of 0.63 nm^2;[45] R=1.0 nm for gA is from Nielsen et al.,[60] which is also consistent from radial lipid densities obtained from MD simulations of gA in assorted bilayers.[61] Hence, there was no fitting for Set I. It is evident from Fig. 4 (top) that the Set I parameters capture the trends of all three systems and provide qualitative agreement for DPPC, but yield poor agreement for the gA monomer and dimers.

Sets II and III involved fitting using the diffusion constants from simulations carried out with the PR integrator; diffusion constants from WC simulations are included in Fig. 4, but were not used for the fits. Fitting for Set II (Fig. 4, middle) considers a change in the hydrodynamic radii for DPPC and gA. It is well known experimentally, by comparing diffusion/sedimentation to partial specific volumes for globular proteins in solution, that a layer of bound water must be included when estimating a hydrodynamic radius;[15] the occupancy of this hydration layer does not need to be 100% because of screening.[62] The slightly lower average diffusion constants of DPPC in the mixtures with gA dimers also imply some interaction of peptide and lipid, and the need to increase the effective hydrodynamic radius of each species. Consequently, R for both DPPC and gA was allowed to vary independently for the fitting of Set II, with an upper bound of the increase set to the

diameter of DPPC, 0.9 nm. The new radii are listed in Table 5, and the substantial improvement in agreement between simulation and the model is shown in the middle panel of Fig. 4. Set III attempts to model the confinement of water near the bilayer surface by allowing variation in η_f and R. Interestingly, the effective radius of DPPC equals the value from Set I, based on surface area. In effect, the slight increase in lipid friction can be modeled by a small increase in R or η_f for DPPC. The effective radius of gA is also smaller for Set III than Set II, but is still approximately a lipid radius larger than Set I.

The present modeling focused on the simulations carried out with the PR integrator. Hence, the agreement of diffusion constants from the WC simulations with the parameters in Table 5 is only semi-quantitative. Excellent agreement may be obtained by increasing the viscosities ($\eta_m = 1.26 \times 10^{-8}$ P·cm and $\eta_f = 0.016$ P) while maintaining b and R to the values in Table 5, Set I (fit not shown). This is to be expected from the damping intrinsic to the WC method.

3.2.2. Extrapolating to infinite system size.—The results presented so far clearly demonstrate the extent of PBC effects for even a coarse-grained model, where the Saffman-Delbrück lengths (see Table 5) are not dramatically larger than the simulation cells (Table 2). As illustrated by Fig. 1 (for all-atom simulations), in the absence of a hydrodynamic model it is virtually impossible to predict the infinite size value D^{∞} of an object diffusing in a bilayer from a simulation. This situation is hence qualitatively different from estimating diffusion constants in a homogenous system: while a model can be used to extrapolate to infinite size,[3] it is possible in practice to keep increasing the size of a cubic box to obtain the limiting value. (This is not always to case for non-cubic boxes as elaborated by Vögele and Hummer.[6]) However, the good agreement of the PSD model and the simulation data for Sets II and III of Table 5 and Fig. 4 supports the notion that the diffusion constants *can* be extrapolated to infinite size provided values for η_m, b, η_f, and R are available. The results are listed in the last rows of Table 5. As expected from the Saffman-Delbrück lengths, the PBC corrections are not very large for largest box size (L = 25.2 nm) listed in Table 3: 22%, 29%, and 39% for DPPC, gA monomer, and gA dimer, respectively.

For the present case, the extrapolation was easily carried out because values of η_m, b, and η_f for DPPC were provided by den Otter and Shkulipa.[59] Nevertheless, a substantial adjustment to R for gA is critical, and a small adjustment to η_f improves the fits slightly. While the viscosity for pure solvent is easy to obtain from simulation, estimating η_m and b is not routine. Hence, it is necessary to consider the errors in the extrapolation.

The Appendix presents a Bayesian method using a single measured (simulated) value of D^{PBC}, system size, the hydrodynamic parameters, and their uncertainties, and provides examples of how the uncertainties effect the predictions of D^{∞} for a membrane spanning peptide. Here the methodology is applied to the diffusion constants of Martini DPPC from the NVE simulations of 512 and 2048 lipids, using web-based interface provided in the link https://diffusion.lobos.nih.gov/bayes.html. Uncertainties in D are set to those obtained in the simulations, and to 2% for H and L (see Table 2). The hydrodynamic parameters are those for Set I in Table 5, with uncertainties of 5% for η_m and η_f, 25% for R, and 100% for b. For convenience, diffusion constants are reported in units of 10^{-7} cm^2/s, and the 95% confidence

interval (CI) follows in parentheses. The extrapolations for N=512 and 2048 yield D^{∞} = 12.7 (12.4–13.1) and 12.3 (12.1–12.6), respectively. R = 0.49 (0.39–0.61) nm and 0.51 (0.40–0.66) for N=512 and 2048, respectively. This increase from 0.45 might be expected because the parameters for Set I in Table 5 yield D^{∞} = 13.1; the increased hydrodynamic radius leads to a slightly lower diffusion constant. The D^{∞} and R calculated here are similar to those of Set II of Table 5, which were obtained from a fit of the Martini NPT simulations of DPPC and gA dimers and monomers.

3.3. All-Atom Simulations.

3.3.1. Comparison with the Periodic Saffman-Delbrück model.—

The expense of all-atom simulations severely limits a comparison of size dependence because the range of L is small and the statistical errors are high. Nevertheless, the trajectories generated on Anton provide an opportunity because all are at least a μs. An added complication of the analysis is that, in contrast to Martini DPPC, independent values of η_m and b are not available. This problem was circumvented by using η_m as a fitting parameter; because the diffusion constant is relatively insensitive to b (see Section 3.3.2), b was set to 10^7 P/cm.[63] Fig. 5 plots the diffusion constants for DPPC and DOPC, and the results of fits to η_m for the PSD model (see Figure caption and Table 6 for details). The trend for DPPC is clearly captured by the PSD model (Fig. 5, solid line), but the level of agreement with simulation for N=648 ($L \approx 15$ nm) is poor. It is possible that the relatively large correction for bilayer center of mass diffusion for the N = 72 and 144 systems has confounded the modeling. For this reason fitting was carried out using only the values at N=288 (dotted line), where the relative corrections for bilayer COM diffusion were lower. This leads to agreement of the model and simulation for N=648. Only a single Anton-based result at N = 288 ($L \approx 10$ nm) is available for DOPC; a fit of this point also leads to agreement with the N = 648 point for this lipid.

As in the preceding subsection, extrapolations were carried out using the Bayesian analysis from individual values of D^{sim}. Because η_m and b were not obtained independently, their uncertainties were increased to 500% following the logic of case B of the Appendix. The uncertainties were set to 2% for H and L, 5% η_f (an independent value is available), and 25% for R, as in the previous subsection. The values of D^{∞} from the Bayesian fits (last row of Table 6) are close to the single point fits (5% for DPPC and 9% for DOPC), and the 95% CI bound them. However, the large range of the CI highlights the need for independent estimates of η_m and b.

3.3.2. Comparison of simulated lipid diffusion constants and experiment.—

Diffusion constants from a variety of all-atom simulations of DPPC and DOPC have already been presented in Table 3 and Fig. 5. This subsection considers the extent of their agreement with experiment (D^{exp}).

There are two approaches for comparing diffusion data from simulation to experiment using the PSD model. The first extrapolates simulated values to L, $H \rightarrow \infty$ using Eq. (3b), as already done for the Martini (Tables 5) and all-atom (Table 6) simulations. Using the Bayesian estimates from Table 6, $D^{\infty} = 4.8{-}6.6 \times 10^{-7}$ cm^2/s for DPPC, and $D^{\infty} = 2.0{-}2.7$

$\times 10^{-7}$ cm^2/s for DOPC. From the values of D^{exp} listed in Table 7, D^{∞} is too large by a factor of more than 3 for DPPC, and more than 2 for DOPC. These differences are well beyond the statistical error of the simulated quantities. It should be noted that there is considerable variation in the experimental values for diffusion constants of lipids, particularly DPPC where numerous measurements using bulky spin probes were published in the 1970s.[66–67] These are in the range 3–5 $\times 10^{-8}$ cm^2/s, and are typically lower than values obtained more recently.[68] In contrast, measurements in black lipid membranes[69] yielded approximately 1×10^{-7} cm^2/s. However, in *all* cases these values are substantially lower than either obtained directly from simulation, or extrapolated to infinite system size.

The second approach is to obtain η_m and related quantities from experiment, and insert them into Eq (3a) to calculate the expected diffusion constant for the system size of the simulation; this, in effect, sets a target for the simulation. Sources for η_m could be a direct measurement, or, as is more common, an estimate using D^{exp} and the Saffman-Delbrück model or one its extensions. The analysis below focuses on N=288 (L ≈ 10 nm).

Table 7 indicates that the simulated diffusion constants for DPPC are approximately 35% higher than experiment, and are quite close to experiment for DOPC. D^{sim} for DPPC obtained from the simulation with Langevin dynamics for temperature control (see Table 3) equals experiment. As is already clear from the preceding estimate, these results are fortuitous.

Given the general unavailability of η_m and b for most fluid phase homogenous lipid bilayers, values of η_m were determined from Eq. (3b) by setting $D^{\infty} = D^{exp}$ for 3 fixed values of b, and the viscosity of pure water at the temperature of the experiment. These physical parameters and the size information (Table 3) yield D^{PBC} listed in the column of Table 7. Assuming that both the hydrodynamic model and the FF are close to correct, these results indicate that D for DPPC and DOPC should underestimate experiment by nearly a factor of 3 for simulations of 288 lipids. The conclusion is relatively insensitive to the interleaflet friction; i.e., varying b by an order of magnitude in each direction while maintaining D^{exp} as a target leads to a less than 25% variation in D^{PBC} for the two lipids.

As is evident from Fig. 6, the PSD model implies an effective “variational principle” for diffusion constants obtained from all-atom simulations using system sizes presently possible: they are invariably lower than the infinite size value. Hence, if the methodology (particularly the FF) is correct, simulated diffusion constants are expected to *underestimate* experiment. Conversely, if simulated diffusion constants are close to or larger than experiment, something is incorrect with the methodology.

Hence, both routes of analysis yield the same conclusion. Extrapolating D^{sim} to infinite size yields diffusion constants 2–3 times larger than D^{exp}. Extrapolating D^{exp} to the system sizes of the simulation indicates that D^{sim} should be 3–4 times smaller than obtained. These results imply a problem with the simulation methodology.

It is not unreasonable to suspect the FF. C36, used for all of the all-atom simulations presented here, was primarily developed using equilibrium properties including lipid surface areas, area compressibilities, and NMR order parameters.[14, 72] More recent validations have included mechanical properties such as bending constants and spontaneous curvatures for planar,[65, 73] and inverse hexagonal[74] phases. Agreement with the preceding experiments is excellent, and independent comparisons of C36 with other lipid FF are very favorable.[75–76] Hence, the relative balance of forces between the membrane surface and interior is arguably well captured by C36, at least for equilibrium properties. Dynamical properties such as ^{13}C and ^{31}P NMR T_1 relaxation times of DPPC for C36 also agree well with experiment,[14, 77] but these measurements mostly probe rotational diffusion of individual lipids at the frequencies examined, and not translational diffusion. The viscosity of alkanes was evaluated when developing C27r,[78] a precursor to C36, and agreement with experiment was very good. However, the viscosity of the alkanes comprising the membrane interior is quite low compared to the effective membrane bulk viscosity and is not the primary determinant of lipid diffusion.

There is in fact, a well-known error associated with the C36 FF: the use of TIP3[53] water model, which was slightly modified to the TIP3P[54] version run in most simulations with the CHARMM FFs. The adaption of Ewald summation removed an artifact in TIP3P associated with a cutoff on the electrostatic forces,[79] but further reduced the already too-low viscosity. The viscosity of TIP3P is lower than experiment by a factor of 2–3, depending on the temperature.[64] However, replacing the experimental viscosity for that of TIP3P water (second block of results for each lipid in Table 7) has a negligible effect on D^{PBC} and only a slightly larger one (10–17%) on. Hence, the FF errors inferred here are only indirectly related to the bulk viscosity for TIP3P water. It is likely that the interactions at the water/lipid interface have a stronger influence on the lipid diffusion constant, and that replacing the water model will improve agreement with experiment.

Given that it will not be possible to obtain diffusion constants from all-atom simulations without substantial PBC effects for the foreseeable future, what are the options? First, the system size should be clearly specified when reporting diffusion constants obtained from simulation. Simulations at several different values of L and H would also provide a measure of robustness, assurance that the hydrodynamic regime has been entered, and provide data for extracting hydrodynamic parameters.

Next, the value (with a confidence interval) for infinite size should be included for more quantitative studies, even when not comparing with experiment. For example, from the analysis in Section 3.2.2, $D^{\infty} = 12–13 \times 10^{-7}$ cm^2/s for DPPC at 323 K in the Martini coarse-grained model. Likewise, $D^{\infty} = 4.8–6.6 \times 10^{-7}$ cm^2/s for the C36 all-atom FF DPPC. A comparison of these two values removes the effects of PBC and allows a more focused view on the underlying physics of the models.

As already discussed in Section 3.2.2, a more direct assessment of the hydrodynamic properties of bilayers through simulations might be carried out by calculating the surface viscosity and interleaflet friction directly using techniques such as those proposed by den Otter and Shkulipa.[59] For all-atom studies, the value of could also be obtained from Eqs.

(2b) or (3b) and compared with experiment. Potential target data for η_m may be obtained in Honerkamp-Smith et al.,[80] Petrov and Schwille,[22] Camley and Brown,[63] Dimova et al.,[81] and Camley et al..[82]

4. CONCLUSIONS

As a precursor to the main results of this study, both coarse-grained and all-atom simulations of DPPC bilayers demonstrated that diffusion constants from NVE and NPT simulations are very similar, provided that a high-quality extended system method is used to maintain temperature and pressure. It is possible that longer simulations will reveal statistically significant differences among the simulations (e.g., NVE vs NPT, CHARMM vs Anton), but the differences are, practically speaking, small. The weak-coupling algorithm tends to reduce diffusion constants slightly (Table 2). Temperature control using Langevin dynamics leads to more severe reductions (Table 3).

The preceding results enabled a simulation-based analysis of the Periodic Saffman-Delbrück (PSD) model using different simulation programs and methods. Coarse-grained and all-atom MD simulations of pure lipids at different cell lengths L (and mostly constant heights) show clearly that the calculated diffusion constants of lipids in bilayers contain a significant periodic boundary effect (Tables 2 and 3, and Figs. 4 and 5), as do simulations of gramicidin A (gA) dimers and monomers in DPPC bilayers (Table 4 and Fig. 4). As also shown in Fig. 4, the PSD model provides very good fits to the gA dimer and monomer systems in DPPC, as well as pure DPPC, provided that the hydrodynamic radii of these species are adjusted to take into account “solvent binding” (Table 5, Set II), or the solvent viscosity is increased to model water binding at the membrane surface (Table 5, Set III).

The PBC effects predicted by the PSD model are substantial for all-atom simulations with system sizes presently accessible. Diffusion constants of medium-sized membrane proteins in fluid phase bilayers are expected to be underestimated by factors of 5–10 (Table 1 and Fig. 1), and lipids by a factor of 3–4 (Table 7 and Fig. 6), assuming that the simulation methodology (especially the force field) is correct. Demonstrating agreement with PSD model is difficult for all-atom systems given the range of sizes that can be studied and the large statistical errors of diffusion constants from trajectories on the 100 ns time scale. Nevertheless, the μs simulations presented here clearly indicate a strong PBC effect in the 5–10 nm range for L (Table 3 and Fig. 5), and qualitative agreement with the PSD model; long simulations at larger L will be required for a more satisfactory test of the model. Simulations at fixed L (9.5 nm) showed the expected lack of dependence for 3 values of H (Table 3). Much larger values of H (not presently practical with all-atom MD) will be required to test thoroughly the dependence on this variable.

Given the preceding results it is essential to consider the effects of PBC when comparing the results of all-atom simulations and experiment. Hence, the diffusion constants obtained here for systems of 288 DPPC and DOPC from the CHARMM36 FF are disquieting because they are so close to experiment. If all of the components of the FF and the PSD model were correct, the simulated diffusion constant of DPPC would have been a factor of 4 lower than observed and that of DOPC a factor of 3 lower. Clearly the value of the diffusion constant

should be included as a target for future development of lipid FF, but the effects of finite system sizes must not be ignored. Experimental values of membrane surface viscosities and interleaflet friction may also provide valuable targets for simulation.

The substantial periodic boundary condition errors in diffusion constants for membrane lipids and proteins in coarse-grained and especially all-atom studies make it especially important that estimates of D^{∞} are reported along with the simulated values. The estimate can be involved: independent determination of the membrane surface viscosity η_m and interleaflet friction b, and simulations at multiple values of L and H. Or it can be quite simple: a single point determination of the surface viscosity and a reasonable assumption for b. The Bayesian analysis presented in the Appendix allows the assignment of confidence intervals for the extrapolated values. Conversely, the absence of an estimate of D^{∞} and its confidence interval substantially diminish the value of a simulated diffusion constant.

Acknowledgements

We thank Klaus Gawrisch, Wouter den Otter, Gerhard Hummer, Edward Lyman, John Howell, Martin Karplus, John Nagle, and Stephanie Tristram-Nagle for helpful discussions, and John Legato for assistance with establishing the diffusion website. This research was supported by the Intramural Research Program of the NIH, National Heart, Lung and Blood Institute, and by the National Science Foundation (Grants No. CHE-1465162 and ACI-1440689), and used the high-performance computational capabilities at the National Institutes of Health, Bethesda, MD (NHLBI LoBoS and Biowulf clusters). Anton computer time was provided by the National Center for Multiscale Modeling of Biological Systems (MMBioS) through Grant P41GM103712-S1 from the National Institutes of Health and the Pittsburgh Supercomputing Center (PSC). The Anton machine at PSC was generously made available by D.E. Shaw Research. Additionally, computer access was granted from SURFsara (www.surfsara.nl) through The Netherlands Organization for Scientific Research (NWO).

Appendix. Extrapolation of simulated diffusion constants

Review of Theory.

The diffusion constant of a protein or lipid at infinite system size, D^{∞}, is the appropriate quantity to compare with experiment or different simulations. From Eqs. (2b) and (3b), it is evident that D^{∞} can be obtained from the membrane surface viscosity η_m, the viscosity of the external fluid η_f, the hydrodynamic radius of the inclusion, R, and (for lipids and monotopic peptides) the interleaflet friction b; i.e., the diffusion constant calculated directly from the simulation, D^{sim}, is not, in principle, required. Unfortunately, η_m and b are difficult to calculate, and have only been obtained directly from simulation for a few systems;[59, 83] even R is difficult to set *a priori* because of partially bound solvent lipids and water. This Appendix shows how these parameters can be extracted from D^{sim} using Bayesian statistics, and discusses the uncertainties and errors associated with extrapolating a single diffusion constant to the infinite system limit.

The Bayesian inference in this case utilizes the limited direct information (a single simulated diffusion constant, D^{sim}), and the confidence in the expected ranges of the parameters η_m, η_f, b, R (for notational convenience these parameters are denoted by the single symbol θ). Formally, the parameters θ are expected to be observed with prior probability $q(\theta)$. The goal is to compute the posterior distribution of these parameters; i.e., the probability of these

parameters given the observation D^{sim}: $p(\theta|D^{sim})$. By Bayes' theorem, $p(\theta|D^{sim}) \propto p(D^{sim}|\theta)q(\theta)$. Here, $p(D^{sim}|\theta)$ is the likelihood that D^{sim} would be observed if the true parameters were θ. For simplicity $p(D^{sim}|\theta)$ is assumed to be a normal distribution with mean $D^{PBC}(\theta)$ given by Eq. (2a) or (3a) as appropriate for the parameters θ, and standard deviation σ_D. Computing $p(\theta|D^{sim})$ analytically is not possible because the dependence in $D^{PBC}(\theta)$ is complex. Therefore, a simple Monte Carlo rejection method was used to estimate $p(\theta|D^{sim})$.[84] The procedure is:

1. Generate a proposed set of parameters θ_{prop} according to the prior distributions $q(\theta)$;
2. Compute $D^{PBC}(\theta)$;
3. Accept this parameter set with probability $exp\left(\frac{-\left[D^{PBC}(\theta) - D^{sim}\right]^2}{2\sigma_D^2}\right)$.

After many iterations of steps (1) to (3) (200,000 was used here), the distribution of accepted parameters yields an estimate of the posterior probability $p(\theta|D^{sim})$. This method is one of the simplest possible, and could be accelerated in many ways,[84] but is sufficient for this application.

As an example, consider the diffusion of a 1 nm radius transmembrane protein in DPPC in Martini at 323 K. For a system with L = 20 nm, H = 5 nm, Eq. 2a predicts that $D^{PBC} = 4.45 \times 10^{-7}$ cm^2/s, and $D^{\infty} = 7.40\times 10^{-7}$ cm^2/s by Eq. 2b. If the simulation has statistical errors of 1% ($\sigma_D = 0.044$ cm^2/s) it would not be surprising if $D^{sim} = 4.4 \times 10^{-7}$ cm^2/s. The measurement will now be analyzed in two different ways: A) with the knowledge of the Martini DPPC viscosities at 323 K, and B) only knowing the rough order of magnitude of these numbers. The convention used the text will be used here as well: D is expressed in units of 10^{-7} cm^2/s and followed by the 95% confidence intervals (CI) in parenthesis.

A) From Den Otter and Shkulipa, [59] $\eta_m = 1.2 \times 10^{-8}$ Poise cm, and $\eta_f = 0.007$ Poise (the values used in much of the text). Allowing for some small errors in these values, the priors are chosen to be log-normal with means given by the measured viscosities and standard deviations of 5% of the mean. R is assumed to have a log-normal distribution with mean 1 nm, but standard deviation 25% of its mean; here the uncertainty arises from the possibility that the hydrodynamic radius could be slightly different from the geometric radius because of the local boundary conditions. Fig. A1 shows the resulting posterior distributions from a run of n = 200,000 iterations. Unsurprisingly, the predicted $D^{\infty} = 7.35$ (7.16, 7.54) is tightly bounded and only slightly lower than the correct answer of 7.40. It is lower because the hypothetical simulated diffusion constant was set to be slightly lower than D^{PBC}. R also remains close to the assumed value of 1 nm. However, setting $D^{sim} = 4.0$ (from 4.4) yields $D^{\infty} = 7.29$ (6.57, 7.93), and the average value R = 1.5 nm. Hence, high precision estimates of the parameters increase the predictive value of the simulation (plots not shown).

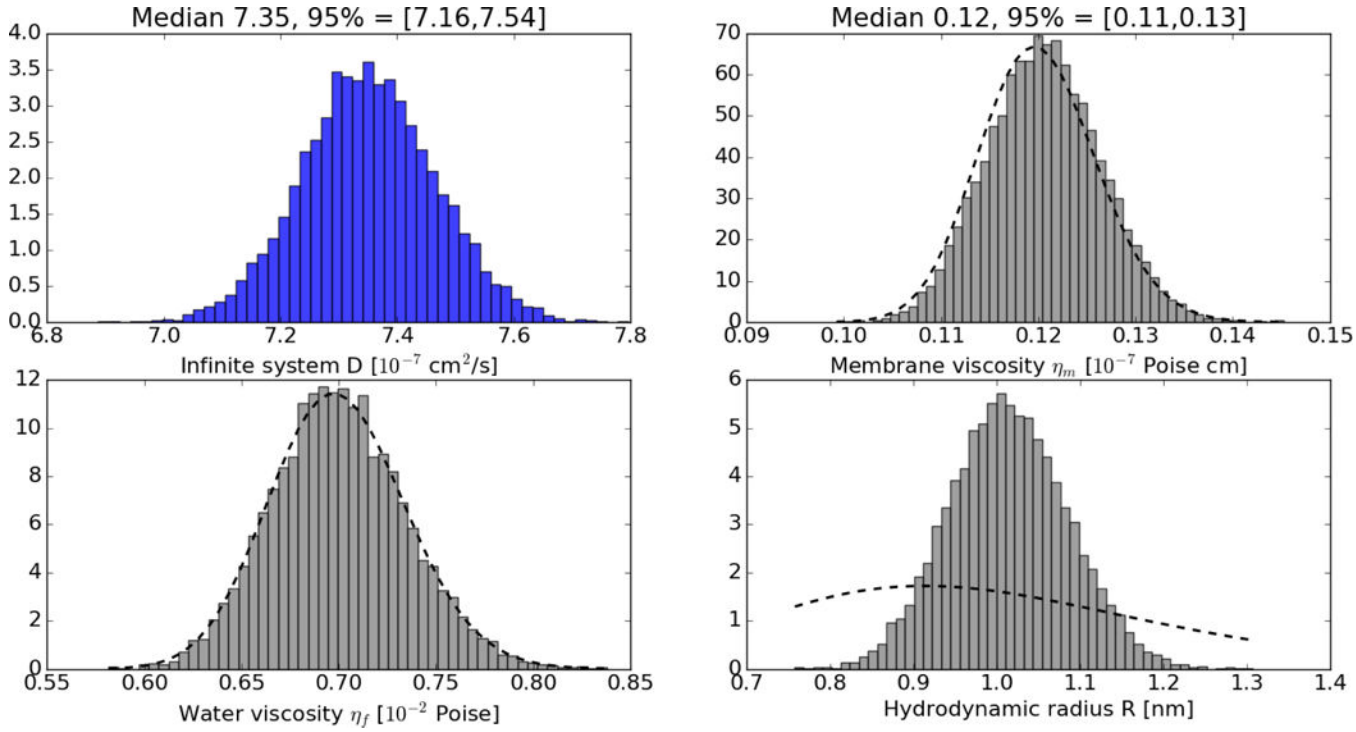

Figure A1.

Posterior distributions for the infinite system D and the parameters of the model, with tightly constrained membrane viscosity and water viscosity (case A). Extrapolating from a single measured diffusion coefficient to infinite system diffusion coefficient is very accurate in this case, and the posterior accurately picks out the correct hydrodynamic radius (*R*). Histograms are normalized to integrate to one, and the dashed line indicates the prior distribution for each quantity.

B) If the Martini viscosities were not available, one might still have a sense of the broad range of the viscosity. For this second example, the mean of η_m is set to 4×10^{-8} Poise cm (almost 4 times the previous mean) and standard deviation to 500% of the mean (a very wide variation).

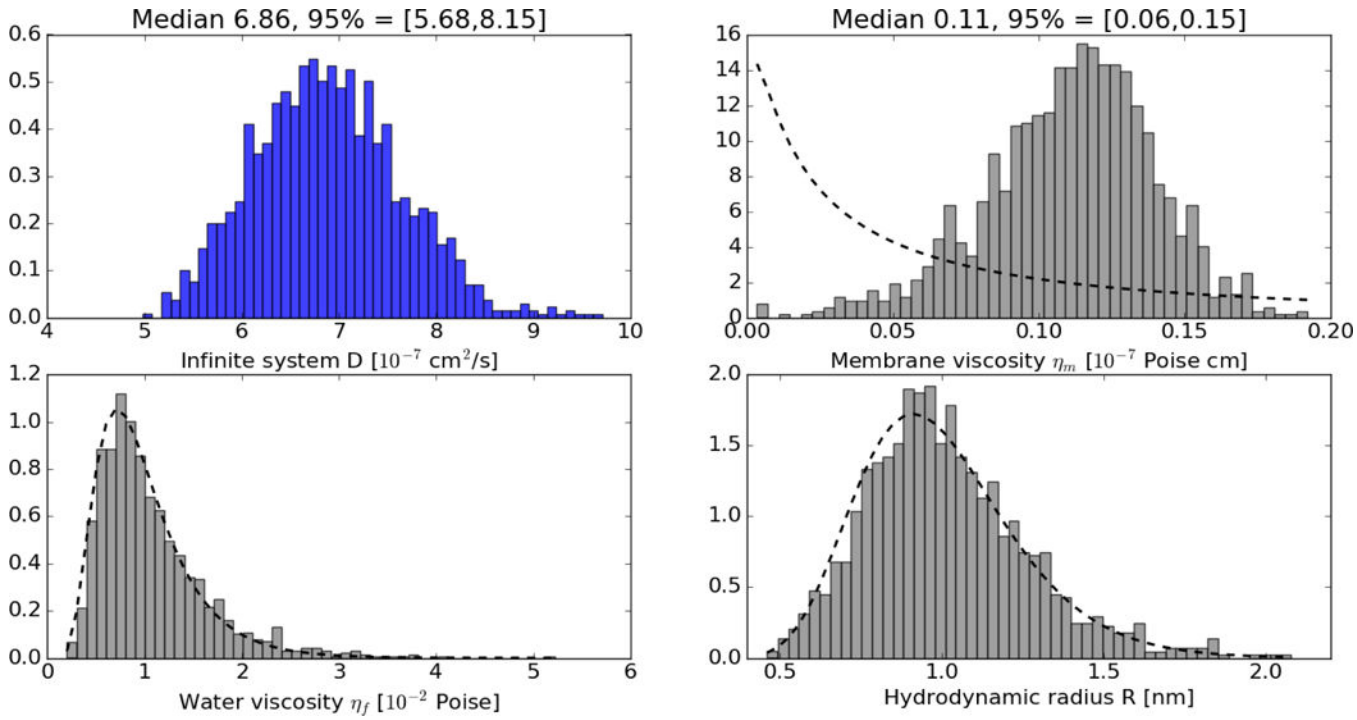

Figure A2.

Posterior distributions for the infinite system D and the parameters of the model, with loosely constrained membrane viscosity and water viscosity (case B). Extrapolating from a single measured diffusion coefficient to infinite system diffusion coefficient allows only rough accuracy here, but the posterior correctly picks out a reasonable membrane viscosity. However, no additional information is gained on the inclusion radius. Histograms are normalized to integrate to one, and the dashed line indicates the prior distribution for each quantity. (Note that because the priors are broader, many fewer proposed parameters are accepted, and these histograms are noisier than those in Fig. A1, even though both come from Monte Carlo runs of n = 200,000 iterations).

The water viscosity is set to 0.01 Poise, with a 50% uncertainty (water viscosities are known to vary less from system to system than membrane viscosities). The assumptions pertaining to R remain unchanged from case A. As shown in Fig A2, these priors yield D_∞ = 6.86 (5.59–8.15). While the 95% CI still brackets the true value, there is significantly more uncertainty than the statistical error in D^{sim} (1%). Nevertheless, this corresponds to a remarkable improvement over the 500% uncertainty in the viscosity initially assumed.

The approach that outlined here has been generalized to allow variation of system length and height, and the interleaflet friction, as required to treat monotopic proteins or lipids (see example in the main text). The following link provides a web-based implementation of the approach https://diffusion.lobos.nih.gov/bayes.html.

References

1. Hasimoto H, On the Periodic Fundamental Solutions of the Stokes Equations and their Application to Viscous Flow Past a Cubic Array of Spheres. J. Fluid Mech. 1959, 5 (2), 317–328.

2. Dunweg B; Kremer K, Molecular Dynamics Simulation of a Polymer Chain in Solution. J. Chem. Phys. 1993, 99 (9), 6983–6997.

3. Yeh IC; Hummer G, System-Size Dependence of Diffusion Coefficients and Viscosities from Molecular Dynamics Simulations with Periodic Boundary Conditions. J. Phys. Chem. B. 2004, 108 (40), 15873–15879.

4. Camley BA; Lerner MG; Pastor RW; Brown FLH, Strong Influence of Periodic Boundary Conditions on Lateral Diffusion in Lipid Bilayer Membranes. J. Chem. Phys. 2015, 143, 243113. [PubMed: 26723598]

5. Saffman PG; Delbruck M, Brownian Motion in Biological Membranes. Proc. Natl. Acad. Sci. U. S. A. 1975, 72 (8), 3111–3113. [PubMed: 1059096]

6. Vogele M; Hummer G, Divergent Diffusion Coefficients in Simulations of Fluids and Lipid Membranes. J. Phys. Chem. B 2016, 120 (33), 8722–8732. [PubMed: 27385207]

7. Vaz WLC; Criado M; Madeira VMC; Schoellmann G; Jovin TM, Size Dependence of the Translational Diffusion of Large Integral Membrane-Proteins in Liquid-Crystalline Phase Lipid Bilayers - A Study Using Flourescence Recovery After Photobleaching. Biochemistry 1982, 21 (22), 5608–5612. [PubMed: 6216914]

8. Weiss K; Neef A; Qui V; Kramer S; Gregor I; Enderlein J, Quantifying the Diffusion of Membrane Proteins and Peptides in Black Lipid Membranes with 2-Focus Fluorescence Correlation Spectroscopy. Biophys. J. 2013, 105 (2), 455–462. [PubMed: 23870266]

9. Ramadurai S; Holt A; Krasnikov V; van den Bogaart G; Killian JA; Poolman B, Lateral Diffusion of Membrane Proteins. J. Am. Chem. Soc. 2009, 131 (35), 12650–12656. [PubMed: 19673517]

10. Gambin Y; Lopez-Esparza R; Reffay M; Sierecki E; Gov NS; Genest M; Hodges RS; Urbach W, Lateral Mobility of Proteins in Liquid Membranes Revisited. Proc. Natl. Acad. Sci. U. S. A. 2006, 103 (7), 2098–2102. [PubMed: 16461891]

11. Naji A; Levine AJ; Pincus PA, Corrections to the Saffman-Delbruck Mobility for Membrane Bound Proteins. Biophys. J. 2007, 93 (11), L49–L51. [PubMed: 17872958]

12. Kriegsmann J; Gregor I; von der Hocht I; Klare JP; Engelhard M; Enderlein J; Fitter J, Translational Diffusion and Interaction of a Photoreceptor and Its Cognate Transducer Observed in Giant Unilamellar Vesicles by Using Dual-Focus FCS. ChemBioChem 2009, 10 (11), 1823–1829. [PubMed: 19551796]

13. Vaz WLC; Hallmann D, Experimental Evidence Against the Applicability of the Saffman-Delbruck Model to the Translational Diffusion of Lipids in Phosphatidylcholine Bilayer Membranes I. FEBS Lett. 1983, 152 (2), 287–290.

14. Klauda JB; Venable RM; Freites JA; O'Connor JW; Tobias DJ; Mondragon-Ramirez C; Vorobyov I; MacKerell AD, Jr.; Pastor RW, Update of the CHARMM All-Atom Additive Force Field for Lipids: Validation on Six Lipid Types. J. Phys. Chem. B 2010, 114 (23), 7830–7843. [PubMed: 20496934]

15. Van Holde KE, Physical Biochemistry, Second Edition Prentiss Hall: Englewood Cliffs, NJ, 1885.

16. Niemela PS; Miettinen MS; Monticelli L; Hammaren H; Bjelkmar P; Murtola T; Lindahl E; Vattulainen I, Membrane Proteins Diffuse as Dynamic Complexes with Lipids. J. Am. Chem. Soc. 2010, 132 (22), 7574–7575. [PubMed: 20469857]

17. Allen MP; Tildesley DJ, Computer Simulations of Liquids. Clarendon Press: Oxford, 1987.

18. Darden T; York D; Pedersen L, Particle Mesh Ewald - an NLog(N) Method for Ewald Sums in Large Systems. J. Chem. Phys. 1993, 98 (12), 10089–10092.

19. Cicuta P; Keller SL; Veatch SL, Diffusion of Liquid Domains in Lipid Bilayer Membranes. J. Phys. Chem. B 2007, 111 (13), 3328–3331. [PubMed: 17388499]

20. Peskin CS, The Immersed Boundary Method. Acta Numerica 2002, 11, 479–517.

21. Hughes BD; Pailthorpe BA; White LR, The Translational and Rotational Drag on a Cylinder Moving in a Membrane. J. Fluid Mech. 1981, 110 (SEP), 349–372.

22. Petrov EP; Schwille P, Translational Diffusion in Lipid Membranes Beyond the Saffman-Delbruck Approximation. Biophys. J. 2008, 94 (5), L41–L43. [PubMed: 18192354]

23. Levine AJ; MacKintosh FC, Dynamics of Viscoelastic Membranes. Phys. Rev. E 2002, 66 (6).

24. Naji A; Brown FLH, Diffusion on Ruffled Membrane Surfaces. J. Chem. Phys. 2007, 126 (23).

25. Reister-Gottfried E; Leitenberger SM; Seifert U, Hybrid Simulations of Lateral Diffusion in Fluctuating Membranes. Phys. Rev. E 2007, 75 (1).
26. Domanski J; Marrink SJ; Schafer LV, Transmembrane Helices can Induce Domain Formation in Crowded Model Membranes. Biochimica Et Biophysica Acta-Biomembranes 2012, 1818 (4), 984–994.
27. Javanainen M; Hammaren H; Monticelli L; Jeon JH; Miettinen MS; Martinez-Seara H; Metzler R; Vattulainen I, Anomalous and Normal Diffusion of Proteins and Lipids in Crowded Lipid Membranes. Faraday Discuss. 2013, 161, 397–417. [PubMed: 23805752]
28. Goose JE; Sansom MSP, Reduced Lateral Mobility of Lipids and Proteins in Crowded Membranes. PLoS Comput. Biol. 2013, 9 (4).
29. Jeon JH; Javanainen M; Martinez-Seara H; Metzler R; Vattulainen I, Protein Crowding in Lipid Bilayers Gives Rise to Non-Gaussian Anomalous Lateral Diffusion of Phospholipids and Proteins. Phys. Rev. X 2016, 6 (2).
30. Oppenheimer N; Diamant H, Correlated Diffusion of Membrane Proteins and Their Effect on Membrane Viscosity. Biophys. J. 2009, 96 (8), 3041–3049. [PubMed: 19383450]
31. Henle ML; Levine AJ, Effective Viscosity of a Dilute Suspension of Membrane-Bound Inclusions. Phys. Fluids 2009, 21 (3).
32. Happel J; Brenner H, Low Reynolds Number Hydrodynamics with Special Applications to Particulate Media. Kluwer: The Hague, 1983.
33. Camley BA; Brown FLH, Fluctuating Hydrodynamics of Multicomponent Membranes with Embedded Proteins. J. Chem. Phys. 2014, 141 (7), 075103. [PubMed: 25149817]
34. Abney JR; Scalettar BA; Owicki JC, Self-Diffusion of Interacting Membrane Proteins. Biophys. J. 1989, 55 (5), 817–833. [PubMed: 2720077]
35. Bussell SJ; Koch DL; Hammer DA, Effect of Hydrodynamic Interactions on the Diffusion of Integral Membrane Proteins - Tracer Diffusion in Organelle and Reconstituted Membranes. Biophys. J. 1995, 68 (5), 1828–1835. [PubMed: 7612824]
36. Marrink SJ; de Vries AH; Mark AE, Coarse Grained Model for Semiquantitative Lipid Simulations. J. Phys. Chem. B 2004, 108 (2), 750–760.
37. Marrink SJ; Risselada HJ; Yefimov S; Tieleman DP; de Vries AH, The MARTINI Force Field: Coarse Grained Model for Biomolecular Simulations. J. Phys. Chem. B 2007, 111 (27), 7812–7824. [PubMed: 17569554]
38. Monticelli L; Kandasamy SK; Periole X; Larson RG; Tieleman DP; Marrink SJ, The MARTINI Coarse-Grained Force Field: Extension to Proteins. J. Chem. Theory Comput. 2008, 4 (5), 819–834. [PubMed: 26621095]
39. de Jong DH; Singh G; Bennett WFD; Arnarez C; Wassenaar TA; Schafer LV; Periole X; Tieleman DP; Marrink SJ, Improved Parameters for the Martini Coarse-Grained Protein Force Field. J. Chem. Theory Comput. 2013, 9 (1), 687–697. [PubMed: 26589065]
40. de Jong DH; Baoukina S; Ingolfsson HI; Marrink SJ, Martini Straight: Boosting Performance Using a Shorter Cutoff and GPUs. Comput. Phys. Commun. 2016, 199, 1–7.
41. Townsley LE; Tucker WA; Sham S; Hinton JF, Structures of Gramicidins A, B, and C Incorporated into Sodium Dodecyl Sulfate Micelles. Biochemistry 2001, 40 (39), 11676–11686. [PubMed: 11570868]
42. Periole X; Cavalli M; Marrink SJ; Ceruso MA, Combining an Elastic Network With a Coarse-Grained Molecular Force Field: Structure, Dynamics, and Intermolecular Recognition. J. Chem. Theory Comput. 2009, 5 (9), 2531–2543. [PubMed: 26616630]
43. Pronk S; Pall S; Schulz R; Larsson P; Bjelkmar P; Apostolov R; Shirts MR; Smith JC; Kasson PM; van der Spoel D; et al., GROMACS 4.5: a High-Throughput and Highly Parallel Open Source Molecular Simulation Toolkit. Bioinformatics 2013, 29 (7), 845–854. [PubMed: 23407358]
44. Brooks BR; Brooks CL; Mackerell AD; Nilsson L; Petrella RJ; Roux B; Won Y; Archontis G; Bartels C; Boresch S; et al., M., CHARMM: The Biomolecular Simulation Program. J. Comput. Chem. 2009, 30 (10), 1545–1614. [PubMed: 19444816]
45. Wassenaar TA; Ingolfsson HI; Bockmann RA; Tieleman DP; Marrink SJ, Computational Lipidomics with *insane*: A Versatile Tool for Generating Custom Membranes for Molecular Simulations. J. Chem. Theory Comput. 2015, 11 (5), 2144–2155. [PubMed: 26574417]

46. Berendsen HJC; Postma JPM; Vangunsteren WF; Dinola A; Haak JR, Molecular Dynamics with Coupling to an External Bath. J. Chem. Phys. 1984, 81 (8), 3684–3690.
47. Bussi G; Donadio D; Parrinello M, Canonical Sampling Through Velocity Rescaling. J. Chem. Phys. 2007, 126 (1).
48. Parrinello M; Rahman A, Polymorphic Transitions in Single-Crystals - A New Molecular Dyanamics Method. J. Appl. Phys. 1981, 52 (12), 7182–7190.
49. Hynninen AP; Crowley MF, New Faster CHARMM Molecular Dynamics Engine. J. Comput. Chem. 2014, 35 (5), 406–413. [PubMed: 24302199]
50. Pickard FC; Miller BT; Schalk V; Lerner MG; Woodcock HL; Brooks BR, Web-Based Computational Chemistry Education with CHARMMing II: Coarse-Grained Protein Folding. PLoS Comput. Biol. 2014, 10 (7).
51. Hoover WG, Canonical Dynamics - Equilibrium Phase-Space Distributions. Phys. Rev. A. 1985, 31 (3), 1695–1697.
52. Nose S, A Unified Formulation of the Constant Temperature Molecular Dynamics Methods J. Chem. Phys. 1984, 81 (1), 511–519.
53. Jorgensen WL; Chandrasekhar J; Madura JD; Impey RW; Klein ML, Comparison of Simple Potential Functions for Simulating Liquid Water. J. Chem. Phys. 1983, 79 (2), 926–935.
54. Durell SR; Brooks BR; Bennaim A, Solvent-Induced Forces between Two Hydrophilic Groups. J. Phys. Chem. 1994, 98 (8), 2198–2202.
55. Nagle JF; Tristram-Nagle S, Structure of Lipid Bilayers. Biochimica et Biophysica Acta-Reviews on Biomembranes 2000, 1469 (3), 159–195.
56. Tristram-Nagle S, Use of X-Ray and Neutron Scattering Methods with Volume Measurements to Determine Lipid Bilayer Structure and Number of Water Molecules/Lipid. Subcell Biochem 2015, 71, 17–42. [PubMed: 26438260]
57. Shaw DE; Dror RO; Salmon JK; Grossman JP; Mackenzie KM; Bank JA; Young C; Deneroff MM; Batson B; Bowers KJ; et al., Millisecond-Scale Molecular Dynamics Simulations on Anton. Proceedings of the Conference on High Performance Computing Networking, Storage and Analysis 2009.
58. Martyna GJ; Tobias DJ; Klein ML, Constant-Pressure Molecular Dynamics Algorithms. J. Chem. Phys. 1994, 101 (5), 4177–4189.
59. den Otter WK; Shkulipa SA, Intermonolayer Friction and Surface Shear Viscosity of Lipid Bilayer Membranes. Biophys. J. 2007, 93 (2), 423–433. [PubMed: 17468168]
60. Nielsen C; Goulian M; Andersen OS, Energetics of Inclusion-Induced Bilayer Deformations. Biophys. J. 1998, 74 (4), 1966–1983. [PubMed: 9545056]
61. Kim T; Lee KI; Morris P; Pastor RW; Andersen OS; Im W, Influence of Hydrophobic Mismatch on Structures and Dynamics of Gramicidin A and Lipid Bilayers. Biophys. J. 2012, 102 (7), 1551–1560. [PubMed: 22500755]
62. Venable RM; Pastor RW, Frictional Models for Stochastic Simulations of Proteins. Biopolymers 1988, 27 (6), 1001–1014. [PubMed: 3401553]
63. Camley BA; Brown FLH, Diffusion of Complex Objects Embedded in Free and Supported Lipid Bilayer Membranes: Role of Shape Anisotropy and Leaflet Structure. Soft Matter 2013, 9 (19), 4767–4779.
64. Venable RM; Hatcher E; Guvench O; MacKerell AD; Pastor RW, Comparing Simulated and Experimental Translation and Rotation Constants: Range of Validity for Viscosity Scaling. J. Phys. Chem. B 2010, 114 (39), 12501–12507. [PubMed: 20831149]
65. Venable RM; Brown FLH; Pastor RW, Mechanical Properties of Lipid Bilayers from Molecular Dynamics Simulation. Chem. Phys. Lipids 2015, 192, 60–74. [PubMed: 26238099]
66. Cullis PR, Lateral Diffusion Rates of Phosphatidylcholine in Vesicle Membranes: Effects of Cholesterol and Hydrocarbon Phase Transitions. FEBS Lett. 1976, 70 (1), 223–228. [PubMed: 992064]
67. Wu ES; Jacobson K; Papahadjopoulos D, Lateral Diffusion in Phospholipid Multibilayers Measured by Fluorescence Recovery After Photobleaching. Biochemistry 1977, 16 (17), 3936–3941. [PubMed: 901758]

68. Lindblom G; Oradd G, Lipid Lateral Diffusion and Membrane Heterogeneity. Biochimica Et Biophysica Acta-Biomembranes 2009, 1788 (1), 234–244.
69. Fahey PF; Webb WW, Lateral Diffusion in Phospholipid Bilayer Membranes and Multilamellar Liquid Crystals. Biochemistry 1978, 17 (15), 3046–3053. [PubMed: 698183]
70. Scheidt HA; Huster D; Gawrisch K, Diffusion of Cholesterol and its Precursors in Lipid Membranes Studied by H-1 Pulsed Field Gradient Magic Angle Spinning NMR. Biophys. J. 2005, 89 (4), 2504–2512. [PubMed: 16085761]
71. Lide DR, CRC Handbook. 81 ed.; CRC Press: Boca Raton, FL, 2000.
72. Pastor RW; MacKerell AD, Jr., Development of the CHARMM Force Field for Lipids. J. Phys. Chem. Letters 2011, 2, 1526–1532.
73. Levine ZA; Venable RM; Watson MC; Lerner MG; Shea J-E; Pastor RW; Brown FLH, Determination of Biomembrane Bending Moduli in Fully Atomistic Simulations. J. Am. Chem. Soc. 2014, 136 (39), 13582–13585. [PubMed: 25202918]
74. Sodt AJ; Pastor RW, Bending Free Energy from Simulation: Correspondence of Planar and Inverse Hexagonal Lipid Phases. Biophys. J. 2013, 104 (10), 2202–11. [PubMed: 23708360]
75. Ollila OHS; Pabst G, Atomistic Resolution Structure and Dynamics of Lipid Bilayers in Simulations and Experiments. Biochimica Et Biophysica Acta-Biomembranes 2016, 1858 (10), 2512–2528.
76. Botan A; Favela-Rosales F; Fuchs PFJ; Javanainen M; Kanduc M; Kulig W; Lamber A; Loison C; Lyubartsev A; Miettinen MS; et al., Toward Atomistic Resolution Structure of Phosphatidylcholine Headgroup and Glycerol Backbone at Different Ambient Conditions. J. Phys. Chem. B 2015, 119 (49), 15075–15088. [PubMed: 26509669]
77. Klauda JB; Roberts MF; Redfield AG; Brooks BR; Pastor RW, Rotation of Lipids in Membranes: Molecular Dynamics Simulation, P-31 Spin-Lattice Relaxation, and Rigid-Body Dynamics. Biophys. J. 2008, 94 (8), 3074–3083. [PubMed: 18192349]
78. Klauda JB; Brooks BR; MacKerell AD; Venable RM; Pastor RW, An Ab Initio Study on the Torsional Surface of Alkanes and its Effect on Molecular Simulations of Alkanes and a DPPC Bilayer. J. Phys. Chem. B 2005, 109 (11), 5300–5311. [PubMed: 16863197]
79. Feller SE; Pastor RW; Rojnuckarin A; Bogusz S; Brooks BR, Effect of Electrostatic Force Truncation on Interfacial and Transport Properties of Water. J. Phys. Chem. 1996, 100 (42), 17011–17020.
80. Honerkamp-Smith AR; Woodhouse FG; Kantsler V; Goldstein RE, Membrane Viscosity Determined from Shear-Driven Flow in Giant Vesicles. Phys. Rev. Lett. 2013, 111 (3).
81. Dimova R; Dietrich C; Hadjiisky A; Danov K; Pouligny B, Falling Ball Viscosimetry of Giant Vesicle Membranes: Finite-Size Effects. European Physical Journal B 1999, 12 (4), 589–598.
82. Camley BA; Esposito C; Baumgart T; Brown FLH, Lipid Bilayer Domain Fluctuations as a Probe of Membrane Viscosity. Biophys. J. 2010, 99 (6), L44–L46. [PubMed: 20858410]
83. Muller TJ; Muller-Plathe F, Determining the Local Shear Viscosity of a Lipid Bilayer System by Reverse Non-Equilibrium Molecular Dynamics Simulations. ChemPhysChem 2009, 10 (13), 2305–2315. [PubMed: 19630053]
84. Gamerman D; Lopes HF, Markov Chain Monte Carlo: Stochastic Simulation for Bayesian Inference. CRC Press: 2006.

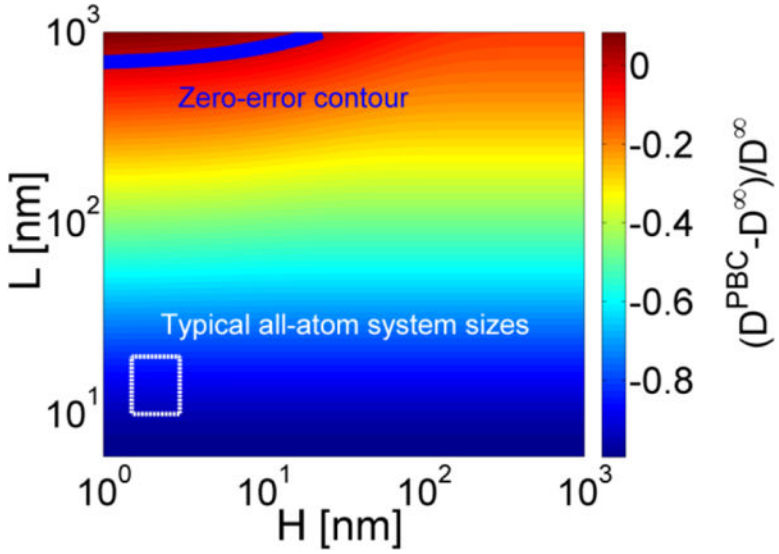

Figure 1.

The relative error in diffusion constants D^{PBC} for a membrane spanning cylinder with radius R = 3 nm in a simulation box with length L and half-water layer thickness H, and Saffman-Delbrück length L_{SD} = 160 nm. This value of L_{SD} is consistent with the experimental diffusion data for proteins determined by Poolman and coworkers.[9] The typical range in nm for all-atom simulation ($10 < L < 20$; $1.5 < H < 3$) is shown with yellow dotted lines. The zero error contour, where $D^{PBC} = D^{\infty}$, is a thick blue line.

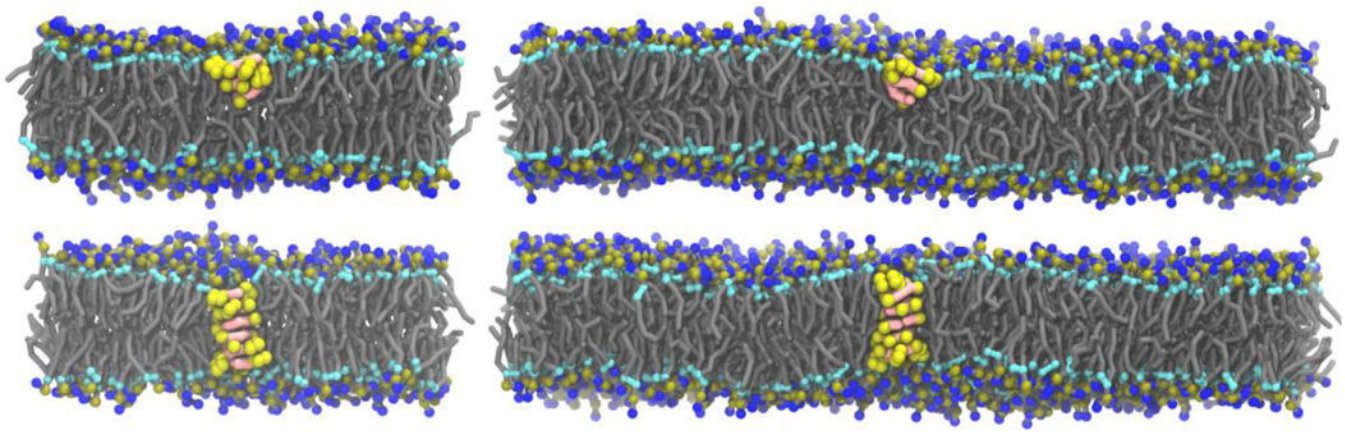

Figure 2.

Coarse-grained systems of gA monomer (top) and gA dimer (bottom) in DPPC bilayers. The dimer systems have 512 (left) and 2048 (right) lipids; the monomer systems contain 6 additional lipids in the lower leaflets. An approximately 13 nm layer of water between periodic images is not depicted to conserve space. Coloring for the beads is: chain gray, glycerol turquoise, phosphate olive green, choline dark blue, gA backbone salmon, gA sidechain yellow.

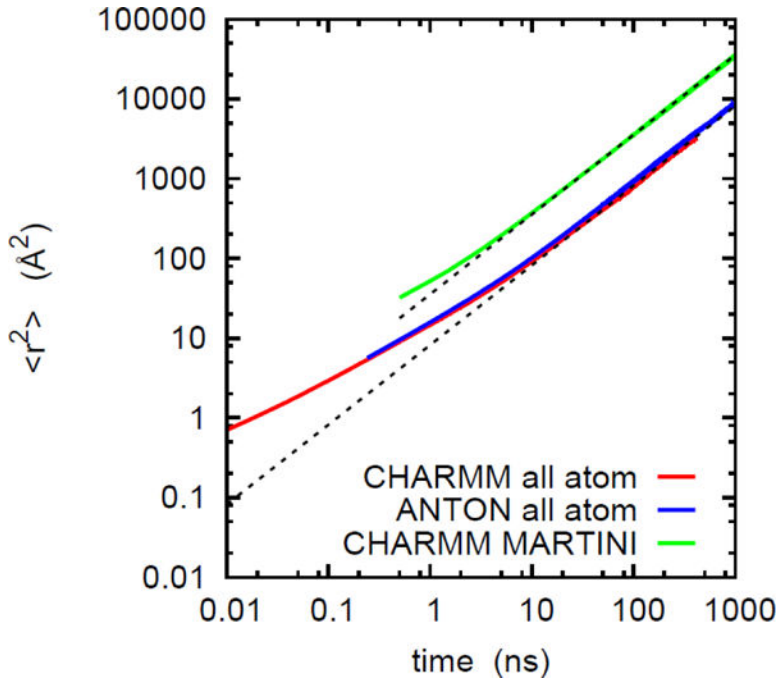

Figure 3.

Log-log plots of mean squared displacement vs time for selected coarse-gained and all-atom simulations. The linear fit for longer time is extrapolated to short time to highlight the subdiffusive regime for the two models.

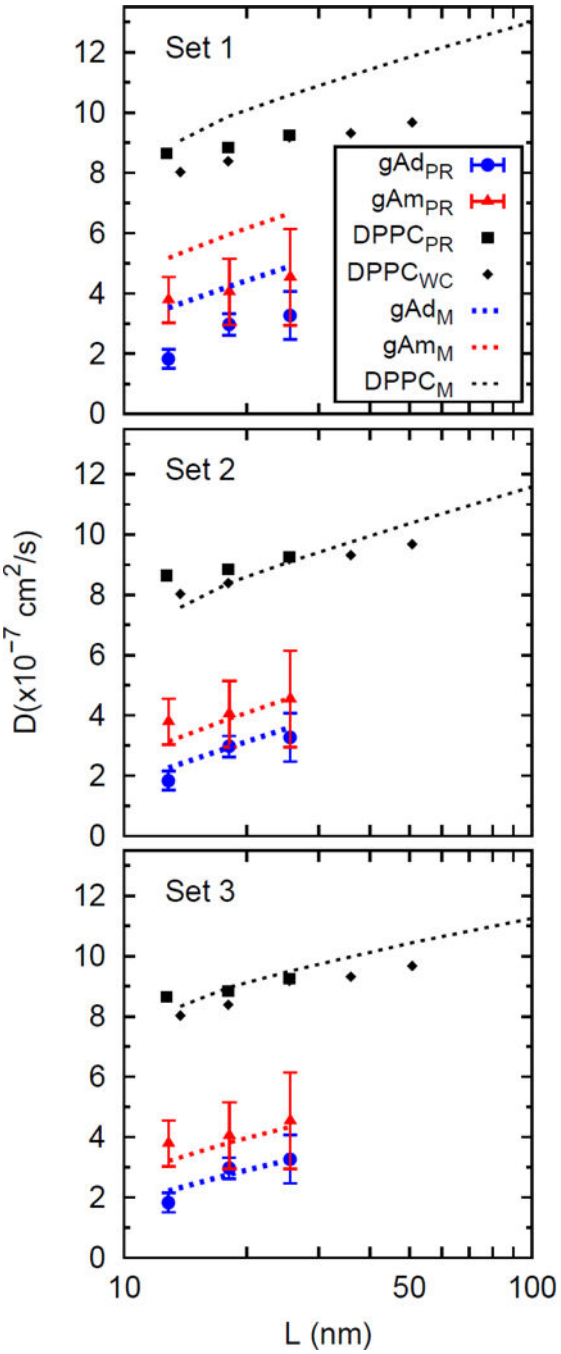

Figure 4.

Diffusion constants from Martini simulations (symbols) and the PSD model predictions (dotted lines) for gramicidin A dimers, monomers, and DPPC vs. *L* with the parameters listed in Table 5 for each Set. Diffusion constants from simulations carried out with weak coupling (WC) were not used for any fitting. Error bars show standard errors; they are comparable to the symbols for the lipids.

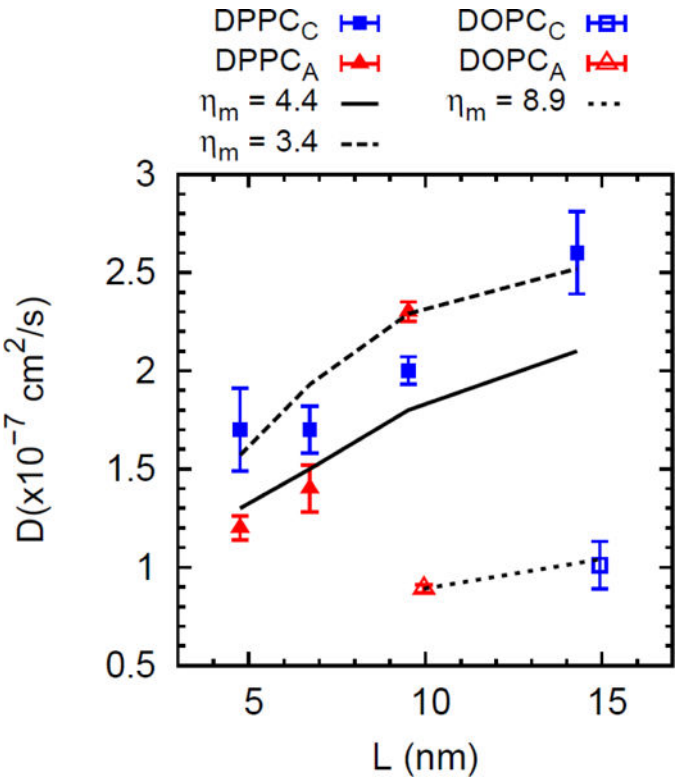

Figure 5.

Diffusion constants from all-atom simulations carried out with Anton and CHARMM for DPPC at 323 K and DOPC at 298 K. The solid line shows the PSD model predictions based on η_m determined by a fit to the diffusion constants from Anton simulations with N = 72 (L = 4.66 nm), 144 (L = 6.60 nm), and 288 (L = 9.60 nm); the dotted lines show PSD model results based only N=288 (L = 9.96 nm). See Table 6 for all fit parameters.

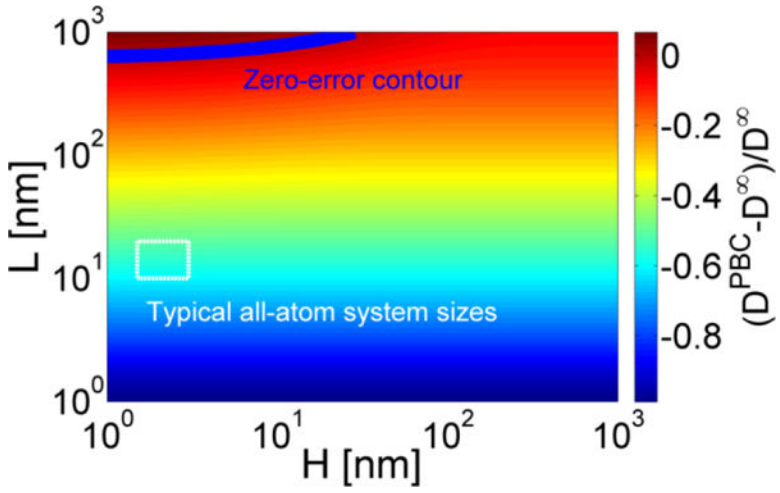

Figure 6.

The relative error in diffusion constants D^{PBC} for a membrane spanning cylinder with radius R = 0.45 nm in a simulation box with length L and half-water layer thickness H, and Saffman-Delbrück length L_{SD} = 146 nm (η_m=1.6 × 10^{-7} P·cm, η_f = 0.00547 P, T=323, b = 1 × 10^{-7} P/cm). The appendix of ref. 4 contains the analogous plot for the Martini model.

Table 1.

D^{∞} and D^{PBC} (in units of 10^{-7} cm^2/s) for three proteins for H=2 nm and L=15 nm, and two values of L_{SD}.

		L_{SD} = 160 nm[a]		L_{SD} = 78 nm[b]	
Protein	**Radius (nm)**	D^{∞}	D^{PBC}	D^{∞}	D^{PBC},[c]
WALP23	0.5	0.605	0.222	1.25	0.519
LacY	2.0	0.467	0.087	0.93	0.203
GltT	4.0	0.398	0.029	0.77	0.068

a) $\eta_m = 3.2 \times 10^{-7}$ P·cm and T=293;

b) $\eta_m = 1.5 \times 10^{-7}$ P·cm and T=323;

c) These entries correct a small error in Table 1 of ref 4, where L and H for the CG example were also used for the all-atom estimates.

Table 2.

Diffusion constants and standard errors (in parentheses) for coarse-grained Martini simulations of DPPC at 323 K for assorted lipid number (N), number of water beads per lipid (N_W), length of simulation box (*L*), half-height of water layer (*H*), and trajectory lengths (T_{run}). Trajectories were carried out with CHARMM (CHM) and GROMACS (GMX) in two different ensembles: NVE and NPT. Temperature and pressure were maintained using standard extended system techniques (see Methods) for CHARMM, and either Parrinello-Rahman (PR) or weak coupling (WC) in GROMACS.

N	N_W	*L* (nm)	*H* (nm)	Program	ensemble	T_{run} (μs)	D (10^{-7}/cm^2/s)
512	23.9	12.70	4.85	CHM	NVE	50	8.62 (0.12)
			4.85	CHM	NPT	50	8.91 (0.15)
	48.9		9.70	CHM	NVE	10	8.69 (0.15)
			9.70	CHM	NPT	10	8.78 (0.17)
	33.3	12.73	6.46	GMX	NPT (PR)	40	8.64 (0.14)
			6.46	GMX	NPT (WC)	40	8.08 (0.09)
1024	31.9	17.99	6.18	GMX	NPT (PR)	40	8.85 (0.07)
		17.99	6.18	GMX	NPT (WC)	40	8.51 (0.08)
2048	23.9	25.40	4.85	CHM	NVE	10	9.81 (0.06)
			4.85	CHM	NPT	10	9.79 (0.07)
	49.6		9.70	CHM	NVE	10	9.63 (0.10)
			9.70	CHM	NPT	10	9.97 (0.26)
	32.0		6.22	GMX	NPT (PR)	40	9.26 (0.10)
			6.22	GMX	NPT (WC)	40	9.08 (0.08)
4096	31.9	35.92	6.19	GMX	NPT (WC)	40	9.30 (0.05)
8192	30.7	50.80	5.98	GMX	NPT (WC)	40	9.72 (0.11)
32768	30.7	101.60	6.00	GMX	NPT (WC)	40	10.50 (0.12)

Table 3.

Diffusion constants and standard errors (in parentheses) from all-atom simulations of DPPC at 323 K and DOPC at 298 K for different lipid number (N), number of waters per lipid (N_W), length of simulation box (*L*), half-height of water layer (*H*), and trajectory lengths (T_{run}). Trajectories were carried out with CHARMM (CHM) and Anton in three different ensembles: NVE, NVT, and NPT. Temperature and pressure were maintained using standard extended system techniques (see Methods), with the exception of the system denoted "NVT (LD)", where Langevin Dynamics was used. Electrostatic interactions were calculated with Particle Mesh Ewald (PME), unless specifically indicated.

Lipid	N	N_W	*L* (nm)	*H* (nm)	Program	ensemble	T_{run} (μs)	D (10^{-7}/cm^2/s)
DPPC	72	30.4	4.76	1.45	CHM	NPT	0.40	1.7 (0.20)
			4.66	1.52	Anton	NPT	7.60	1.2 (0.06)
	144		6.73	1.46	CHM	NPT	0.40	1.7 (0.07)
			6.60	1.52	Anton	NPT	4.00	1.4 (0.12)
	288		9.52	1.46	CHM	NVE(Ewald)	0.50	2.5 (0.19)
					CHM	NVE	0.20	2.0 (0.10)
					CHM	NVT	0.20	2.0 (0.28)
					CHM	NVT (LD)	0.15	1.5 (0.10)
			9.60	1.43	Anton	NPT	1.00	2.3 (0.05)
		15.2	9.49	0.73	CHM	NPT	0.30	1.9 (0.12)
		30.4	9.53	1.46	CHM	NPT	0.40	2.0 (0.07)
		60.8	9.52	2.87	CHM	NPT	0.40	2.1 (0.11)
	648	30.4	14.29	1.46	CHM	NPT	0.10	2.6 (0.21)
DOPC	288	33.5	9.96	1.40	CHM	NPT	0.40	0.93 (0.08)
			9.96	1.40	Anton	NPT	1.00	0.89 (0.02)
	648		14.94	1.41	CHM	NPT	0.15	1.01 (0.04)

Table 4.

Diffusion constants and standard errors (in parentheses) for Martini simulations of gramicidin A (gA) dimers and monomers in bilayers with different numbers (N) of DPPC, number of water beads per lipid (N_W), length of simulation box (*L*), half-height of water layer (*H*), and trajectory lengths (T_{run}). The last column lists the diffusion constants for the lipids in the simulation cell. Trajectories carried out with GROMACS at NPT using Parrinello-Rahman for temperature and pressure control.

peptide	N (DPPC)	N_W	*L* (nm)	*H* (nm)	*D* (peptide) (10^{-7} cm^2/s)	T_{run} (μs)	*D* (DPPC) (10^{-7} cm^2/s)
gA dimer	512	38.7	12.84	7.36	1.83 (0.32)	180	8.34 (0.06)
	1024	31.9	18.09	6.12	2.97 (0.35)	180	8.70 (0.05)
	2048	33.3	25.52	6.41	3.27 (0.80)	180	9.16 (0.04)
gA monomer	518	38.2	12.86	7.34	3.79 (0.76)	180	8.56 (0.10)
	1030	31.7	18.10	6.11	4.05 (1.1)	180	8.86 (0.08)
	2054	33.2	25.54	6.41	4.54 (1.6)	180	9.17 (0.03)

Table 5.

Parameters for fitting diffusion constants from coarse-grained simulations to the Periodic Saffman-Delbrück model: membrane surface viscosity (η_m), leaflet friction (b), fluid bulk viscosity (η_f), hydrodynamic radius (R) of gA monomers and dimers, and the Saffman-Delbruck length (L_{SD}). The last 3 rows list D^{∞} (units of 10^{-7} cm^2/s) for each species calculated from Eqs (2b) and (3b). These extrapolations are discussed further in Section 3.2.2.

Parameter	Set I	Set II	Set III
η_m (10^{-8} P·cm)	1.2	1.2	1.2
b (10^5 P/cm)	2.4	2.4	2.4
η_f (P)	0.007	0.007	0.0139
R (DPPC) (nm)	0.45	0.53	0.45
R (gA) (nm)	1.0	1.72	1.46
L_{SD} (nm)	8.57	8.57	4.32
D^{∞} (DPPC)	13.12	12.27	11.08
D^{∞} (gA monomer)	9.19	6.95	5.86
D^{∞} (gA dimer)	7.40	5.99	4.74

Table 6.

Fitted value of η_m and extrapolated D^∞ (units of 10^{-7} cm^2/s) for 2 extrapolations from diffusion constants obtained from of all-atom simulations on Anton for 3 systems (N=72, 144, and 288) or only 1 (N=288); values of b, η_f and R fixed. The last row lists D^∞ with 95% confidence intervals from the Bayesian method described in the Appendix.

Parameter	DPPC		DOPC
number of systems fit	3	1	1
b (10^7 P/cm)[a]	1	1	1
η_f (P)	0.00252[b]	0.00252[b]	0.00311[c]
R (lipid) (nm)	0.45	0.45	0.47c
η_m (10^{-8} P·cm)	4.4	3.4	8.9
L_{SD} (nm)	87	67	143
D^∞ from fits	4.8	5.8	2.4
D^∞ from Bayesian		5.5 (4.8–6.6)	2.2 (2.0–2.7)

a) ref. 63 and references therein;

b) ref. 64, the viscosity of TIP3P water at 323 K;

c) ref. 64, the viscosity of TIP3P water at 293 K;

d) ref. 65.

Table 7.

Comparison of simulated diffusion constants for DPPC and DOPC for N = 288 with D^{PBC} (model), the extrapolation of the experimental diffusion constant to the system size of the simulation, for a range of hydrodynamic parameters that yield the experimental value at infinite system size, D^{∞} (model).

Lipid	D^{exp} (10^{-7} cm^2/s)	D^{sim} (10^{-7} cm^2/s)	η_m (10^{-7} P·cm)	η_f (P)	b (10^7 P/cm)	D^{∞} (model) (10^{-7} cm^2/s)	D^{PBC} (model) (10^{-7} cm^2/s)
DPPC	1.5[a]	2.3 (0.1)	1.90	0.00547[c]	0.1	1.50	0.640
(323 K)			1.60	0.00547	1.0	1.51	0.584
			1.45	0.00547	10.0	1.50	0.502
			1.90	0.00252[d]	0.1	1.65	0.641
			1.60	0.00252	1.0	1.69	0.586
			1.45	0.00252	10.0	1.69	0.503
DOPC	0.825[b]	0.90 (0.28)	3.34	0.00890[c]	0.1	0.824	0.354
(298 K)			2.83	0.00890	1.0	0.825	0.333
			2.49	0.00890	10.0	0.824	0.287
			3.34	0.00311[d]	0.1	0.927	0.355
			2.85	0.00311	1.0	0.941	0.332
			2.49	0.00311	10.0	0.962	0.288

[a] ref. 70;

[b] ref. 68;

[c] ref. 71;

[d] ref. 64